

## CHAPTER IV

### DEVELOPMENT OF POROUS HYDROXYAPATITE PARTICLES AS CARRIERS OF PROTEINS FOR BONE TISSUE ENGINEERING

#### 4.1 Abstract

Incorporation of proteins by physical absorption within porous Hydroxyapatite (HAp)-based implants has been frequently reported for orthopaedic uses whereas sequential release is hardly properly controlled. This work aims at developing HAp particles as a controlled release carrier of proteins. HAp carriers were synthesized by coprecipitation technique from dicalcium phosphate dihydrate ( $\text{CaHPO}_4 \cdot 2\text{H}_2\text{O}$ , DCPD) and calcium carbonate ( $\text{CaCO}_3$ ). Incorporation of proteins was accomplished during the coprecipitation of the two reactants. Desorption behavior of proteins from HAp particles will be investigated by UV-Visible spectrophotometry.

(**Key-words:** Hydroxyapatite, protein carrier)

#### 4.2 Introduction

Hydroxyapatite (HAp), having a chemical formula  $\text{Ca}_{10}(\text{PO}_4)_6(\text{OH})_2$  is a naturally occurring inorganic constituent of tooth enamel, dentine, bone and other hard tissues of vertebrates. It has been widely used as bone filler, spacer, and bone graft. HAp has been well-recognized as it is an excellent affinity to biological substances such as collagen, proteins, enzymes, cells, and viruses, biocompatible, osteoconductive and bioactive material (Liu, T-Y. *et al.*, 2005). With the osteoconductive properties, HAp ceramic has been also investigated as scaffolds for cell delivery and tissue engineering. In addition, porous hydroxyapatite ceramics have a considerable potential as carriers for controlled drug release (Ijntema, K. *et al.*, 1994), protein delivery agent, catalyst, and absorbent (Li, Y. *et al.*, 2008). The apatite crystal often used to carry drugs or proteins has regularly a stoichiometric composition, i.e.,  $\text{Ca/P}=1.67$  (Liu, T-Y. *et al.*, 2005). The adsorption of protein onto

HAp is important to accelerate tissue healing when placed in vivo (Yang, Q. *et al.*, 2006) in a variety of oral or osseous biological events. HAp has also adsorptive capabilities with respect to proteins and biologically active molecules, such as osteogenic agents and growth factors. Up to now, many methods such as sol-gel, precipitation, hydrothermal, mechano-chemical, spray pyrolysis, freeze-drying and electrochemical deposition have been developed to prepare HAp powders. In these methods, wet chemical process was usually used to prepare HAp powders because it is easy to operate and need not any expensive equipments (Cao, Li-yun, *et al.*, 2005).

The interaction of proteins with hydroxyapatite appeared to depend on the overall protein charge, the number of acidic and basic groups, and the specific protein structure (Ijntema, K. *et al.*, 1994).

The purpose of this study is to fabricate proteins-HAp powder to control the release rate behavior of different proteins.

### 4.3 Experimental Section

#### 4.3.1 Materials

- Dicalcium phosphate dihydrate (DCPD; Fluka, Germany)
- Calcium carbonate (CaCO<sub>3</sub>; Carlo Erba, Italy)
- Tris-base (Tris[hydroxymethyl]amino methane) (Sigma-Aldrich, USA)
- Nitric acid (ACS reagent 69%; J.T.Baker, USA)
- Ovalbumin (OVA; Sigma-Aldrich, USA)
- Gelatin type B (Sigma-Aldrich, USA)
- Bovine serum albumin (BSA; Sigma-Aldrich, USA)
- Sodium phosphate monobasic (NaH<sub>2</sub>PO<sub>4</sub>) and sodium phosphate dibasic (Na<sub>2</sub>HPO<sub>4</sub>; Ajex Finechem, Australia)

#### 4.3.2 Preparation of Protein-Loaded Hydroxyapatite

Calcium hydrogen phosphate dihydrate ( $\text{CaHPO}_4 \cdot \text{H}_2\text{O}$ , DCPD) and calcium carbonate ( $\text{CaCO}_3$ ) were used as precursors of Ca and P to prepare protein-loaded hydroxyapatite. The molar ratios of Ca to P were fixed at 1.67 which mixed with nitric acid 1 mol/l at 75 °C for 1 h under stirring. Then, pour distilled water at room temperature following protein. Ovalbumin (Sigma-Aldrich A-5253), Gelatin type B, Bovine serum albumin (BSA, Aldrich A-3912) and Crude bone protein from pork bone were selected as candidate proteins in this study. The proteins aqueous solution were prepared by dissolving proteins powder or pellet into distilled water for each synthesis. Regulated pH at a constant value, tris(hydroxymethyl) aminomethane. The aggregates were rinsed with the distilled water until pH=7 (DI water was boiled and decarbonated before use) and further centrifuged at 4500 rpm for 10 mins, freezed at -45 °C and lyophilized at -50 °C. The samples were kept in dessicator until used.

#### 4.3.3 Crude Bone Protein preparation

CBP was extracted from the pork bone. In particular, bone was initially washed and cleaned thoroughly in tap water and then sectioned into small pieces with a high speed motor machine. Pieces of bones were further crushed into powder in liquid nitrogen. Then, the as-prepared powder was immersed in 0.6 N HCl at 4 °C. After three days, the bony solution was centrifuged and the supernatant was collected, dialyzed for 48 h and lyophilized. The dry CBP was kept in desiccators until use (Hariraksapitak, *et al.*, 2009).

#### 4.3.4 Characterization

##### 4.3.4.1 *Thermogravimetric Analysis (TGA)*

The relative amount of the proteins associated with the HAp was determined using thermogravimetric analysis, TG-DTA (Perkin Elmer) instrument under  $\text{N}_2$  flow of 5 ml/min. The heating process was conducted from 30-950 °C at a rate of 10 °C/min.

##### 4.3.4.2 *Fourier-transformed infrared spectrophotometer (FT-IR)*

A Thermo Nicolet Nexus<sup>®</sup> 670 Fourier-transformed infrared spectrophotometer (FT-IR) was used to investigate chemical functionalities of

hydroxyapatite powder by the KBr disk method. Hydroxyapatite powders were randomly selected from each group of samples and detected for the FT-IR spectra with a resolution of  $4\text{ cm}^{-1}$  in the range of  $4000\text{-}400\text{ cm}^{-1}$  and were averaged from 32 scans.

#### 4.3.4.3 Autosorb-1

The BET method uses gas with a known adsorption area per 1 g to measure the surface area of samples based on gas quantities adsorbed to the sample surface. Fifty mg of the sample was preheated at  $200\text{ }^{\circ}\text{C}$  for 10 min to remove water and gas completely. Surface areas of HAp particles were analyzed by nitrogen adsorption in a Autosorb-1.

#### 4.3.4.4 Scanning Electron Microscope (SEM)

For the morphological study, hydroxyapatite were mounted on brass stubs, coated with gold using a JEOL JFC-1100 sputtering device, and observed for their microscopic morphology using JEOL JSM-5200 scanning electron microscopy (SEM). For the morphology of the surface, pore size, distribution and also the interconnectivity.

#### 4.3.4.5 Transmission Electron Microscope (TEM)

The microstructural and morphological features of HAp powders were analysed in JEM-2100 operating voltage of 200 kV. Sample for TEM were prepared by air-drying a drop of a sonicated ethanol suspension of particles onto a carbon-coated copper grid and air-dried.

#### 4.3.4.6 Energy Dispersive Spectrophotometer (EDS)

The Ca/P ratio of the hydroxyapatite was studied by the X-ray microanalysis, using the method of Energy dispersive X-ray spectroscopy (EDS). EDS is an analytical technique used for the elemental compositions of the HAp.

#### 4.3.4.7 X-ray Diffraction (XRD)

The phase compositions, crystal shape and size of HAp powders were characterized by X-ray diffraction (XRD) with copper target. Data were collected over the scanning range ( $2\theta$ ) from  $5^{\circ}$  to  $60^{\circ}$  at a scan speed  $2^{\circ}/\text{min}$ .

The average crystallite size of the prepared hydroxyapatite samples was determined using the scherrer equation.

$$D = K \cdot \lambda / \beta \cdot \cos \theta$$

In which D is the average crystallite size (Å), K denotes the shape factor (K=0.9),  $\lambda$  is the X-ray wavelength (for CuK $\alpha$   $\lambda$ =1.5418 Å),  $\beta$  represents the peak at half width (in rad), and  $\theta$  is the Bragg angle of the peak (002 reflection of hydroxyapatite at  $2\theta$ =26 °).

#### 4.3.4.8 UV-Visible Spectrophotometer

Determination of protein by UV/Vis spectrophotometry at 215 nm for Gelatin type B, 280 nm for OVA and BSA and 275 nm for CBP.

#### 4.3.4.9 Zeta potential (ZP)

Zeta potentials (or electrophoretic mobility) of the hydroxyapatite were determined using Zeta-Meter 3.0+ (Zeta-Meter, Inc., USA): Briefly, the suspension of 100 mg hydroxyapatite in 20 ml of deionized water was filled in an electrophoresis cell. Two electrodes were inserted into the cell and connected to the Zeta-Meter 3.0+ unit. Once the electrodes were energized, microspheres were aroused to move toward one electrode. Particles were observed under a microscope for its movement along a specific distance which was indicated by a built in grid. The zeta potential value was detected at a right time point when the microsphere moved to the end. Measurement was repeated 10 times for each preparative condition and the average values were calculated.

#### 4.3.4.10 Particle size distribution

The Malvern Particle size of hydroxyapatite was measured by Mastersizer 2000 a solution of the particles was sonicated in an ultra-sonic bath for 7 min immediately before measurement to ensure separation of particles. A sample of this mixture was injected into the sample cell of the Malvern Mastersizer. The obscuration was between 10 and 30 %, as required by the instrument. The Mastersizer calculates automatically the particle size and distribution from small angle light scattering using Mie theory and Fraunhofer diffraction theory. The measurements were taken with the stirrer in the Mastersizer to ensure even distribution of particles and prevent sedimentation in the sample cell. Shear forces were not a problem in this case as the goal was to measure the primary particle size. A least 10 measurements were recorded and the average value recorded.

#### 4.3.4.11 *In vitro* protein-HAp release test

Proteins-loaded Hydroxyapatite (20 mg) were dispersed in 10 ml 0.1M phosphate buffer saline (PBS) solution at pH 7.4. All samples were incubated in a shaking water bath (70 rpm) at 37 °C. The releasing medium was withdrawn 1 ml and an equal amount of fresh medium was added to maintain a constant volume of the medium. The amount of protein in the sample solution was determined by UV-visible spectroscopy. Absorbance peaks at 280 nm to determine the ovalbumin and BSA concentration, 215 nm to determine the gelatin type B, and 275 nm to determine the crude bone protein. Concentration through the use of a pre-determined standard concentration—intensity calibration curve. An average value was calculated at each time point. The protein content of the encapsulated particles can be described by two quantities in terms of Encapsulating efficiency of protein-loaded hydroxyapatite (EE) and Loading capacity of hydroxyapatite particle (LC), which were determined according to the following equation (Freiberg and Zhu, 2004).

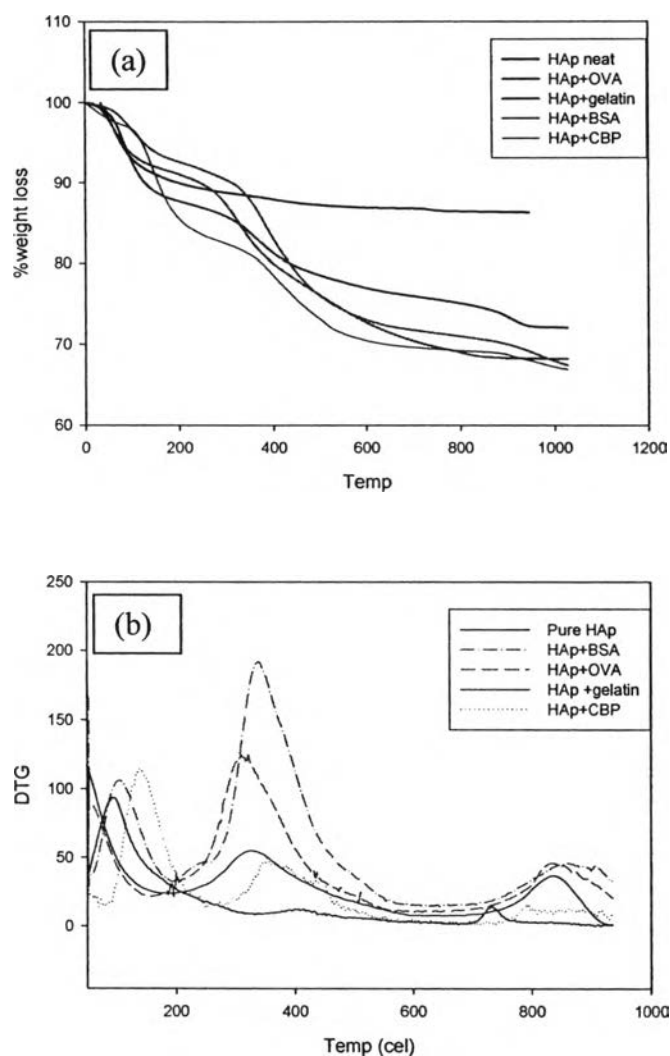
$$\text{Encapsulating efficiency (\%)} = \frac{\text{total mg proteins-encapsulated}}{\text{initial mg proteins-loaded}} \times 100$$

$$\text{Loading capacity (\%)} = \frac{\text{total mg proteins-encapsulated}}{\text{total mg particles}} \times 100$$

## 4.4 Results and Discussion

### 4.4.1 Thermogravimetric Analysis (TGA)

The samples were analyzed by TGA using a Perkin Elmer (TG-DTA) instrument under N<sub>2</sub> flow of 5 ml/min. The heating process was conducted from 30-950 °C at a rate of 10°C/min. To investigate amount of proteins-loaded hydroxyapatite.



**Figure 4.1** TGA-DTG curves (a) TGA, (b) DTG of proteins-loaded hydroxyapatite.

The features of TGA and DTA profiles of proteins-loaded hydroxyapatite were presented in Figure 4.1. The weight loss could be differentiated into three regions in the investigated temperature range such as (i) 25-210 °C, (ii) 210-570 °C, and (iii) 750-950 °C. In the first region of 25-210 °C, the weight loss for all precursors could be attributed to the removal of physically absorbed water. The second region of 210-570 °C is a major weight loss, probably due to the combustion of proteins residuals (organic matter) and with the maximum rate at 350 °C, and decomposition of calcium hydroxide and carbonate to water and carbon dioxide. The

third region of 750-950 °C, the weight loss can be assigned to the decomposition of carbonate compounds.

The TGA curves of the samples (Figure 4.1) show differences in the amount of protein weight loss. Weight loss of ovalbumin was 16.8 %, Gelatin type B was 10.22 %, BSA was 20.61 % and CBP from pork bone was 22 %.

#### 4.4.2 UV-Visible Spectrophotometer

Take water after finish synthesis reaction measured by UV-Visible to determine the remaining protein after reaction. OVA and BSA were measured the wavelength with 280 nm, Gelatin type B with 215 nm and CBP from pork bone with 275 nm.

To investigate amount of proteins-loaded hydroxyapatite. Remaining OVA in the DI water is 6.12 %, Gelatin type B is 14.30 %, and BSA is 2.38 %. So, OVA, Gelatin type B, and BSA are entrapped in hydroxyapatite 20.26 %, 12.08 %, and 24% respectively. It is possible that protein may be lost during the washing HAp with DI water about 5-6 times to become neutral.

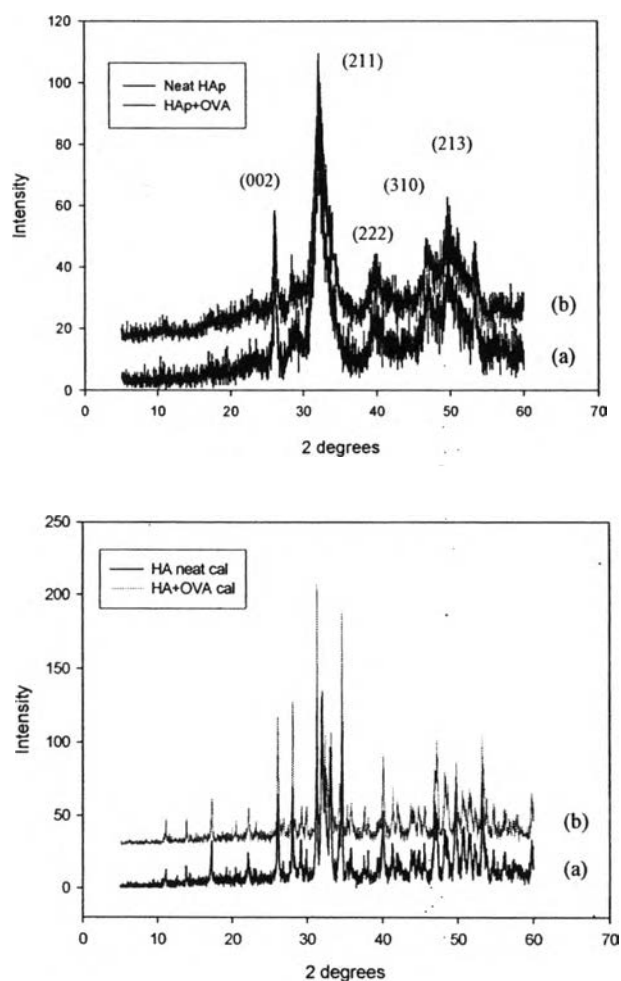
#### 4.4.3 X-ray Diffraction

In the X-ray diffraction analysis, all synthesized precipitates showed a HAp-like pattern (Figure 4.2). The crystallinity of each precipitate was evaluated from the data of the inverse of half value breadth of the (002) peak of HAp (Figure 4.2). The crystallinity of HAp depends on its synthesized temperature in such a way that HAp synthesized at low temperature has low crystallinity. The solubility of HAp also depended on its synthesized temperature and HAp synthesized at low temperature showed high solubility (Matsumoto, T. *et al.*, 2004).

For HAp powders, the crystallite size in a direction perpendicular to the crystallographic plane is always estimated according to Scherrer's formula as followed:

$$d = (0.9\lambda) / \text{FWHM} * \text{Cos}\theta$$

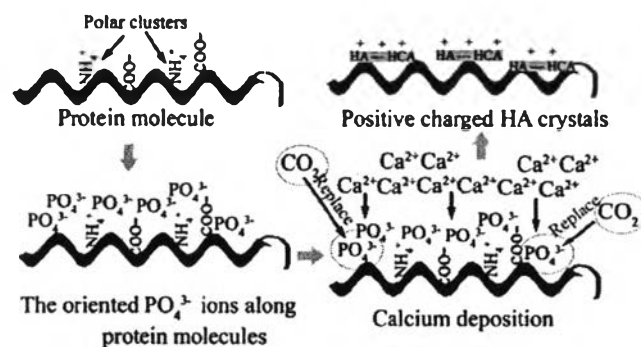




**Figure 4.2** XRD pattern of HAp powders : (a) Neat HAp; (b) OVA-loaded HAp.

where  $d$  is the crystallite size (nm);  $\lambda=0.15406$  nm for Cu  $K\alpha$  radiation of X-ray beam; FWHM the full width at half maximum for the diffraction peak (rad); and  $\theta$  is the Bragg angle of the (002) diffraction angle ( $^{\circ}$ ). Two major characteristic diffraction peaks could be obtained for all the powdered samples: one closed at  $2\theta$  of  $\sim 26^{\circ}$  and the other broad one at  $\sim 32^{\circ}$ . According to PDF no.01-1008, The uncalcined HAp is shown the broad patterns around at (002) and (211). It indicates that the crystallites were very tiny in nature. The (002) peak ( $2\theta\sim 26^{\circ}$ ) from XRD patterns was chosen for calculating the crystallite size as shown in Table 4.1 since it contains the least overlap of the broadened peaks. It could be found that the crystallite size depends on the size of the particle that observed from SEM.

Crystallite size of calcined HAp powders was larger than uncalcined powder. Figure 4.2 indicated that uncalcined HAp powders were amorphous and did not form CaP crystals, because HAp crystallization is mediated by protein and shown in Figure 4.3.



**Figure 4.3** Schematic illustration of the protein-mediated crystallization of HAp crystals with positive charges (Zhao, H. *et al.*, 2008).

**Table 4.1** The different crystallite size of (a) calcined HAp at 800 °C; (b) uncalcined HAp powder

(a)

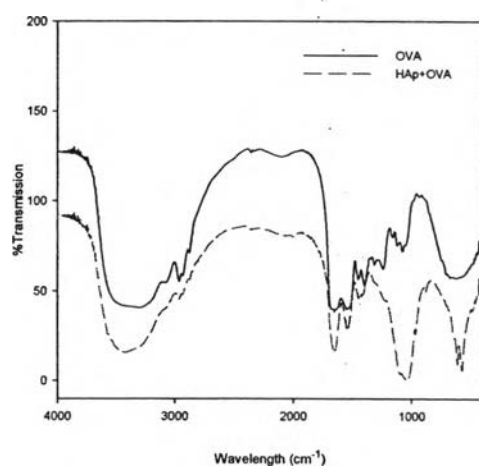
Crystal plane (002)	2θ	FWHM	Crystallite size (nm)
Neat HAp calcine	26.07	0.22	40.01
OVA-HAp calcine	26.05	0.15	58.16
Gealtin-HAp calcine	26.00	0.23	38.37
BSA-HAp calcine	25.82	0.23	37.03

(b)

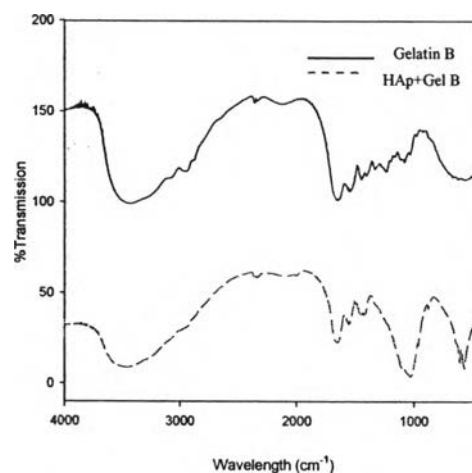
Crystal plane (002)	2θ	FWHM	Crystallite size (nm)
Neat HAp uncalcine	26.11	0.44	20.45
OVA-HAp uncalcine	26.12	0.51	17.69
Gelatin-HAp uncalcine	25.80	0.51	19.37
BSA-HAp uncalcine	25.91	0.51	16.88

#### 4.4.4 Fourier-Transformed Infrared Spectrophotometer

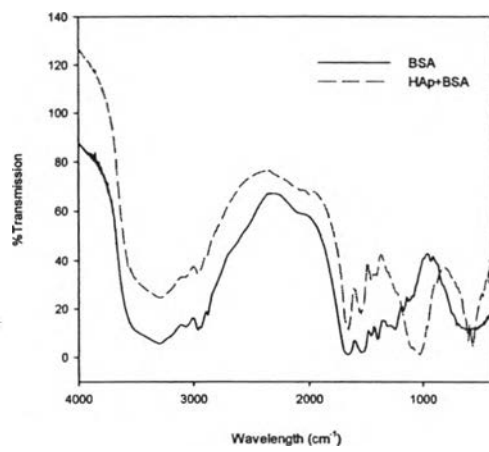
Adsorption of protein on HAp particles was detected by FTIR analysis (Figure 4.4). The spectra show the characteristic peaks of absorbed water, hydroxyl, phosphate and carbonate species. The broad peak around  $3250\text{ cm}^{-1}$  to  $3500\text{ cm}^{-1}$  corresponds to the adsorbed water. The spectrum clearly indicates a peak at  $1640\text{ cm}^{-1}$  which is attributed to the presence of water associated with HAp. The absorption bands at  $1460\text{ cm}^{-1}$  and  $875\text{ cm}^{-1}$  suggest the presence of  $\text{CO}_3^{2-}$ . The absorption bands at  $1040$ ,  $1093$ ,  $962$  and  $571\text{ cm}^{-1}$  detected in the spectra are attributed to the  $\text{PO}_4^{3-}$  ion. The absorption bands at  $1210\text{ cm}^{-1}$  together with one at  $1130\text{ cm}^{-1}$  and clear absorption band at  $879\text{ cm}^{-1}$  are attributed to the  $\text{HPO}_4^{2-}$ . The spectrum of protein exhibited an apparent absorption band at  $1654\text{ cm}^{-1}$  assigned to amide I, C=O stretching mode. The absorption band at  $1540\text{ cm}^{-1}$  assigned to amide II, N-H bending mode and  $1384\text{ cm}^{-1}$  assigned to amide III, C-N stretching mode and N-H bending mode.



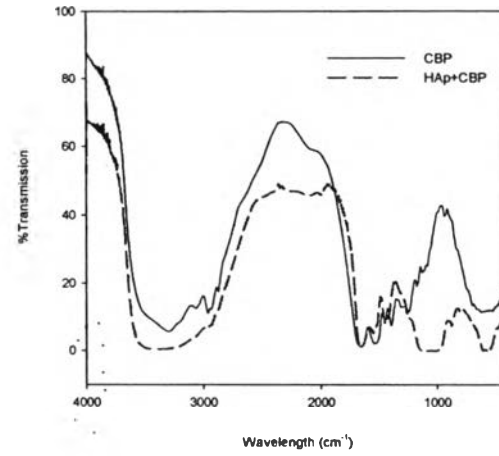
(a)



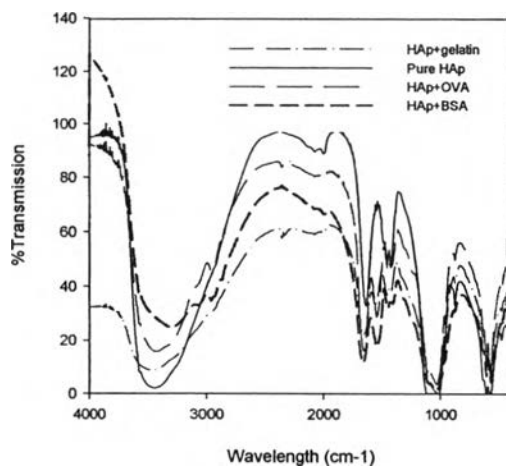
(b)



(c)



(d)



(e)


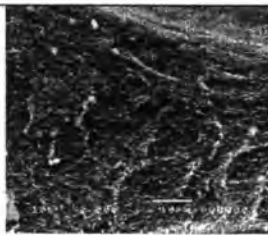
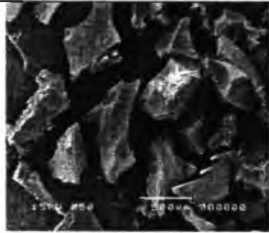
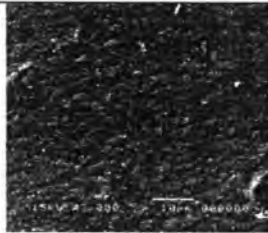

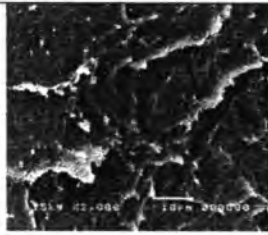
**Figure 4.4** The FTIR spectra of HAp powders of : (a) OVA-loaded HAp; (b) Gelatin-loaded HAp; (c) BSA-loaded HAp; (d) CBP-loaded HAp; (e) including protein/HAp.

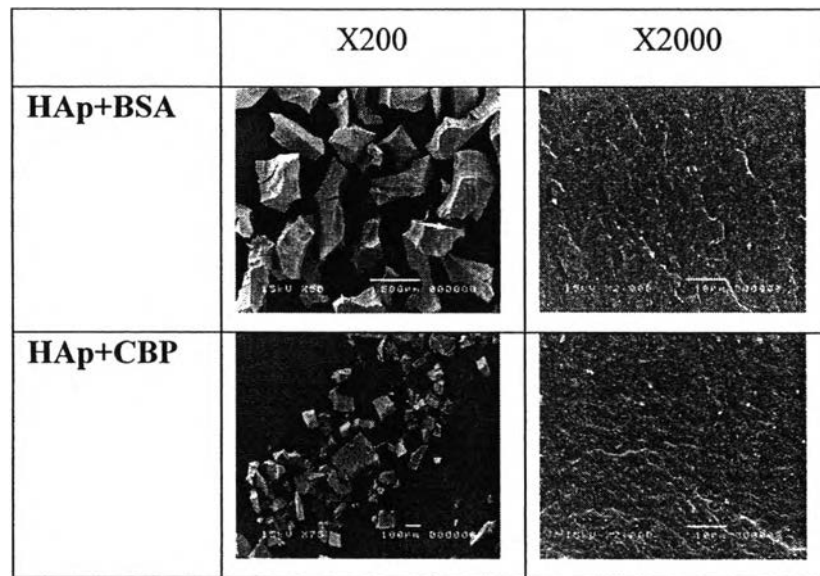
The possible mechanisms can be adapted to explain the interaction between the HAp and proteins molecules. The mechanism can be operated through the electrostatic interaction between the positive  $\text{Ca}^{2+}$  and  $\text{COO}^-$  (protein): this has been also reported by Liu who suggested that there is an intermediate complex between  $\text{COO}^-$  and HAp. This complex can be formed via the electrostatic interaction between the negative  $\text{COO}^-$  on protein molecules and positive  $\text{Ca}^{2+}$  on the C-sites of HAp surface. Kazuhiko K. indicated that the C-sites were located on the crystal planes that are perpendicular to a-axis and b-axis of apatite crystal.

#### 4.4.5 Scanning Electron Microscope (SEM)

To investigate the morphology of HAp powder by using SEM (JEOL, model JEM-5200). It is found that HAp have an arbitrary shape. Some gelatin grafting on the surface of HAp shown in Table 4.2.

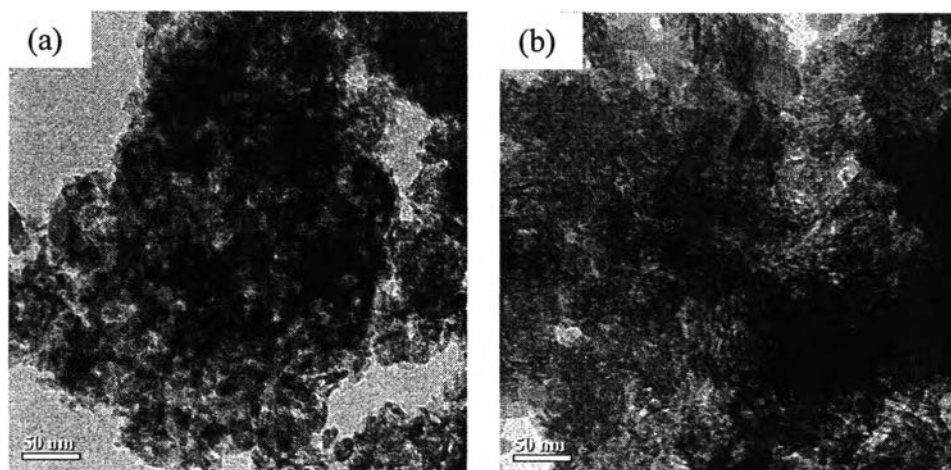
**Table 4.2** SEM of proteins-loaded HAp powder

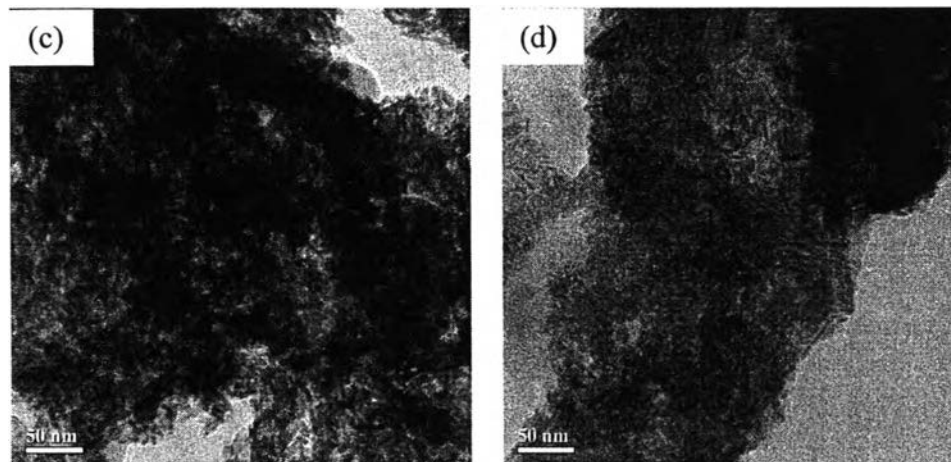
	X200	X2000
<b>Neat HAp</b>		
<b>HAp+OVA</b>		
<b>HAp+gelatin</b>		



#### 4.4.6 Transmission Electron Microscope (TEM)

Figure 4.5 shows the TEM photographs of HAp powders obtained neat HAp and proteins-loaded HAp. The HAp powders contain agglomerated particles consisting of rod-like shaped particle. Neat HAp powders are the short-rod crystal than proteins-loaded HAp. It is found that there are not much differences in morphology and size from the photographs of proteins-load HAp samples.





**Figure 4.5** TEM micrographs of proteins-loaded HAp powder : (a) Neat HAp; (b) OVA-loaded HAp; (c) Gelatin-loaded HAp; (d) BSA-loaded HAp.

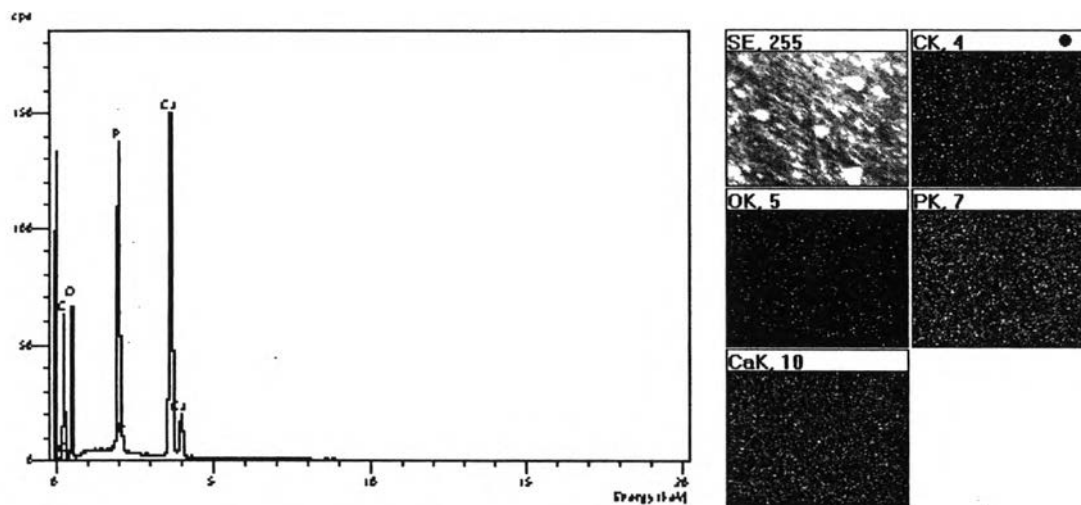
#### 4.4.7 Zeta Potential (ZP).

Twenty milliliter of the suspension was placed in an electrophoresis cup, and the movable images of the particles were recorded by the electrophoresis apparatus. The value would also be beneficial in the study of protein-loaded HAp and releasing through HAp particles. The zeta potentials were measured by applying the electric field in the dispersion and particles in the dispersion will be migrated to electrode of opposite charge. Protein-loaded HAPs were dispersed in the DI water pH about 6-7 if protein can releases from HAp, it will be showed negative charge, so zeta potential is the positive. The zeta potentials of all the samples are negative, indicating that the particles themselves have superfluous positive electrical charges. It was indicated that protein entrapped in the HAp particle

The electrical conductivities values were so close as  $\sim -18$ ,  $-16$ , and  $-20$  mV for neat HAp, OVA-loaded HAp, and Gelatin B loaded HAp particle, respectively. Zeta potential is an indicator of charge density (Brown *et al.*, 1998). Particle size of Gelatin B-loaded HAp is the largest, so it has the highest charge density.

#### 4.4.8 Energy Dispersive Spectrophotometer

The EDS spectrum from HAp particles (Figure 4.6) shows the characteristic peaks of calcium (Ca), phosphorus (P), and oxygen (O). EDS is composed mainly of HAp and exhibits a molar Ca/P ratio of 1.67.



**Figure 4.6** EDS spectrum of the biomimetic apatite layer deposited.

#### 4.4.9 The Brunauer—Emmett—Teller (BET)

Surface areas and pore size of the powders were analyzed by nitrogen adsorption in Autosorb-1. The BET surface areas of the calcined samples at 800 °C are summarized in Table 4.3. We found that they are a few differences in surface area and pore size of neat and proteins-loaded HAp. Pore size of proteins-loaded HAp are a few larger than neat HAp due to the existence of pores after the removal of organic materials (proteins) so, surface area of proteins-loaded HAp are a few lower than neat HAp.

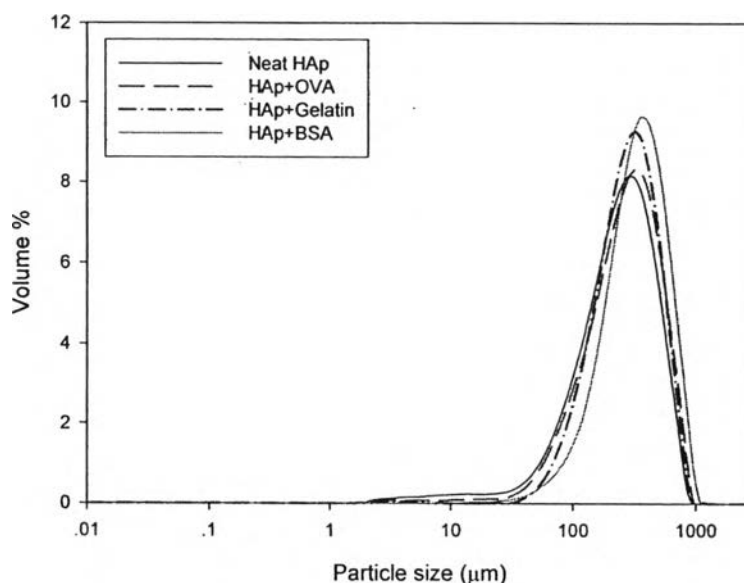


**Table 4.3** BET surface area and pore size of the calcined samples at 800 °C

	Surface area (m <sup>2</sup> /g)	Pore size (nm)
Neat HAp	22.64	8.75
OVA-loaded HAp	19.65	9.35
Gelatin-loaded HAp	20.06	11.42
BSA-loaded HAp	20.99	12.14

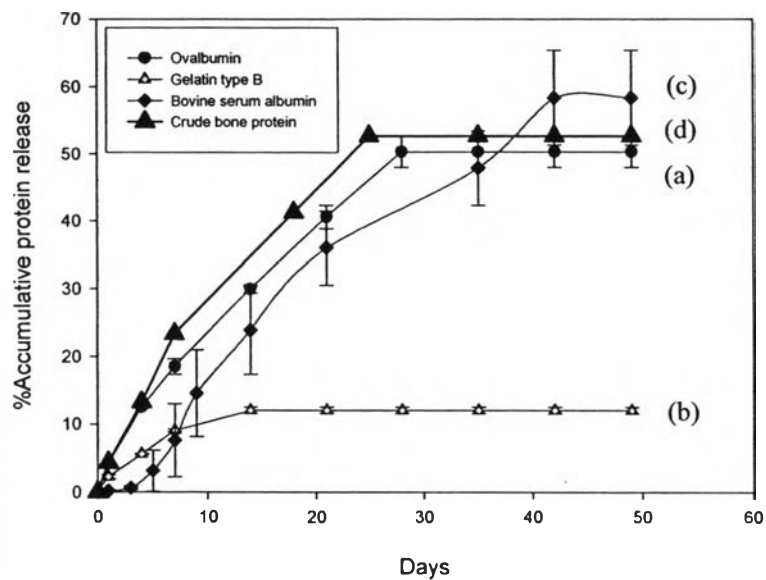
#### 4.4.10 Particle Size Distribution of Hydroxyapatite

We were ground and sieved through a mesh size of 400 micron of protein-loaded HAp particles. About twenty milligrams of HAp were dispersed in water. The size distributions of HAp were measured by light scattering using particle sizer (Malvern, UK). The average particle size distributions of neat HAp and proteins-loaded HAp were about 316  $\mu\text{m}$ .

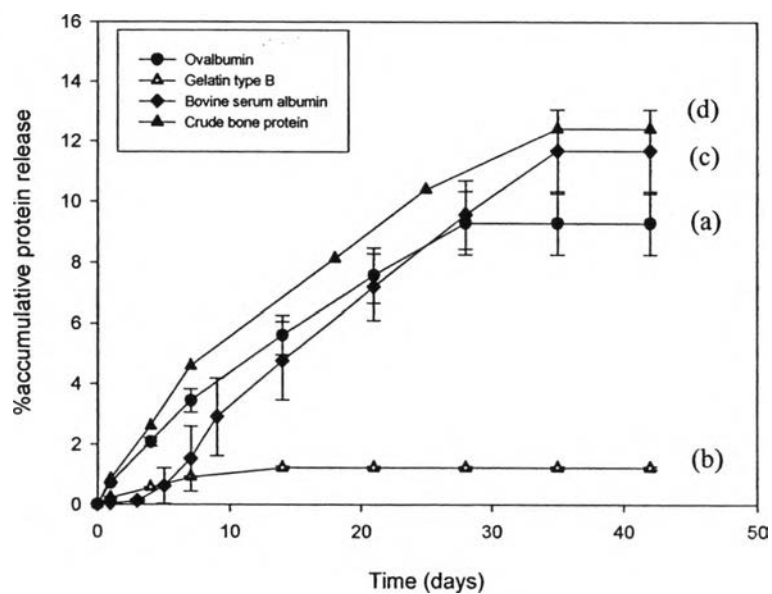
**Figure 4.7** Average particle size distribution of Hydroxyapatite.

#### 4.4.11 Controlled Release of Proteins from HAp Particles

The protein content of the encapsulated particles can be described by two quantities in terms of encapsulating efficiency of protein-loaded hydroxyapatite (EE) and loading capacity of hydroxyapatite particle (LC). For encapsulating efficiency of protein-loaded hydroxyapatite (EE), the proteins release from hydroxyapatite in phosphate buffer saline solution pH 7.4 was shown in Figure 4.8. The release profile of OVA, BSA and CBP were shown long-term proteins release at least 3 week. The maximum accumulative releases were about 50 % - 60 %. For the release profile of gelatin type B, it was shown the bursting release. The accumulative release was about 12 %. For loading capacity of proteins-loaded hydroxyapatite (LC), the proteins release from hydroxyapatite in phosphate buffer saline pH 7.4 was shown in Figure 4.9. The LC of OVA, BSA, and CBP from HAp particles were shown maximum accumulative releases were about 8-12 %. For the LC of Gelatin type B from HAp particle was shown maximum accumulative releases was about 1 %. Encapsulation of proteins into hydroxyapatite particles in this study was on the basis of polyion complexation. It was expected that a degree of molecular interaction was able to take place between proteins and hydroxyapatite particles of opposite charges (Young *et al.*, 2005); as a consequence, a higher yield of the ionic complexes should result in higher encapsulation efficiency and loading capacity (Tabata and Ikada, 1998; Hoffman, 2002; Young *et al.*, 2005).



**Figure 4.8** Encapsulating efficiency of protein-loaded hydroxyapatite (EE) : (a) Ovalbumin (OVA); (b) Gelatin type B; (c) Bovine serum albumin (BSA) and (d) Crude bone protein (CBP) release from HAP in phosphate buffer saline solution.



**Figure 4.9** Loading capacity of protein-loaded HAP (LC) : (a) Ovalbumin (OVA); (b) Gelatin type B; (c) Bovine serum albumin (BSA) and (d) Crude bone protein (CBP) release from HAP in phosphate buffer saline solution.

#### 4.5 Conclusion

The porous hydroxyapatite particle as a controlled release carrier of proteins were successfully synthesized by co-precipitation technique. The precursors were obtained DCPD and  $\text{CaCO}_3$ . Incorporation of proteins was accomplished during the co-precipitation of the two reactants. Characteristics of the HAp particles were determined by XRD, EDS, FT-IR, TGA, ZP, SEM, TEM, and Autosorb-1. Proteins-loaded HAPs were dissolution tested in prolonged PBS solution. Proteins release could be regulated using HAp particles resulting in prolonged release of proteins except gelatin type B. Mechanism of proteins-loaded HAp release was believed to be the combination of diffusion or degradation of the carrier. Many factors play roles and synergistically control on the release of proteins from the hydroxyapatite which were electrostatic interaction between protein and hydroxyapatite.

#### 4.6 Acknowledgements

The author would like to thank Prof. Pitt Supaphol, Assoc. Prof. Prasit Pavasant, Assoc. Prof. Nuanchawee wetprasit, Asst. Prof. Hathaikarn Manuspiya and Dr. Neeranut Kuanchertchoo for their sincere assistances. They have provided the very useful guidance and the great encouragement throughout this research.

The author also thanks to all of colleagues, staff and teachers in the Petroleum and Petrochemical college, Chulalongkorn University who helps greatly during studies.

The author is grateful for funding of the thesis work provided by petroleum and petrochemical college; and Center for petroleum, Petrochemicals, and Advanced Materials.

The author wishes to give thanks to all of friends in Pitt Supaphol group's student for helps and suggestions.

Finally, the author would like to express appreciation for supporting scholarship and caring a great love of family especially mother, father, brother, and grandmother.

#### 4.7 References

- Cao, Li-Yun., Zhang, Chuan-bo., and Huang, Jian-feng (2005). Synthesis of hydroxyapatite nanoparticles in ultrasonic precipitation. Ceramics International, 31, 1041-1044.
- Li, Yanbao., Tjandra, Wiliana., and Tam, Kam C (2008). Synthesis and characterization of nanoporous hydroxyapatite using cationic surfactants as templates. Materials Research Bulletin, 43, 2318–2326.
- Liu, Tse-Ying., Chen, San-Yuan., Liu, Dean-Mo., and Liou, Sz-chian (2005). On the study of BSA-loaded calcium-deficient hydroxyapatite nano-carriers for controlled drug delivery. Controlled Release, 107, 112-121.
- Freiberg, S., Zhu, X.X. (2004). Polymer microspheres for controlled drug release. International Journal of Pharmaceutics, 282, 1-18.
- Hariraksapitak, P. (2009). Development of protein delivery scaffold with a separate drug carrier system for bone tissue regeneration. Doctor dissertation. The Petroleum and Petrochemical College, Chulalongkorn University.
- Hoffman, A.S. (2002). Hydrogels for biomedical applications. Advanced Drug Delivery Reviews, 54(1), 3-12.
- Matsumoto, T., Okazaki, M., Inoue, M., Yamaguchi, S., Kusunose, T., Toyonaga, T., Hamada, Y., and Takahashi (2004). Hydroxyapatite particles as a controlled release carrier of protein. Biomaterials, 25, 3807-3812.
- Kandori, Kazuhiko., Shohei, Oda., Masao, Fukusumi., Yoshiaki Morisada. (2009). Synthesis of positively charged calcium hydroxyapatite nano-crystals and their adsorption behavior of proteins. Biointerfaces, 73, 140-145.
- IJntema, K., HeuveIsland, W.J.M., Dirix, C.A.M.C., and Sam, A.P (1994). Hydroxyapatite microcarriers for biocontrolled release of protein drugs. International Journal of Pharmaceutics, 112, 215-224.
- Tabata, Y. and Ikada, Y. (1998) Protein release from gelatin matrices. Advanced Drug Delivery Reviews, 31(3), 287-301.
- Yang, Qing., Chen, Lin., Shen, Xinyuan., and Tan Zhiqing (2006). Preparation of Polycaprolactone Tissue Engineering Scaffolds by Improved Solvent Casting/Particulate Leaching Method. Macromolecular, 45, 1171-1181.

Young, S., Wong, M., Tabata, Y., and Mikos, A.G. (2005) Gelatin as a delivery vehicle for the controlled release of bioactive molecules. Journal of Controlled Release, 109(1-3), 256-274.

Zhao, Hongshi, He, Wen., Wang, Yingjun., Zhang Xudong., Li, Zhengmao., Yan, Shunpu., Zhou, Weija. Biomimetic (2008). Synthesis and Characterization of Hydroxyapatite Crystal with Low Phase Transformation Temperature. Journal of chemical & engineering data, 53 (12), 2735-2738.